ISSN 1674-1056
http://cpb.iphy.ac.cn
http://iopscience.iop.org/cpb
中国物理 B
Chinese Physics
中国物理 Chinese Physics B

New sulfur-doped source and synergistic effect with nitrogen for carbon dots produced from glucose

Lige Fu(付丽歌)[1], Yuehong Yin(殷月红)[1], Guohua Cao(曹国华)[1], Pingping Wu(武苹苹)[1], Jian Wang(汪舰)[1], Lingling Yan(闫玲玲)[1], Baoqing Zhang(张宝庆)[2], Ming Li(李明)[1]

Citation: Chin. Phys. B . 2019, 28(12): 128102 . **doi:** 10.1088/1674-1056/ab5213
Journal homepage: http://cpb.iphy.ac.cn; http://iopscience.iop.org/cpb

What follows is a list of articles you may be interested in

Large magnetic moment at sheared ends of single-walled carbon nanotubes

Jian Zhang(张健), Ya Deng(邓娅), Ting-Ting Hao(郝婷婷), Xiao Hu(胡潇), Ya-Yun Liu(刘雅芸), Zhi-Sheng Peng(彭志盛), Jean Pierre Nshimiyimana, Xian-Nian Chi(池宪念), Pei Wu(武佩), Si-Yu Liu(刘思雨), Zhong Zhang(张忠), Jun-Jie Li(李俊杰), Gong-Tang Wang(王公堂), Wei-Guo Chu(褚卫国), Chang-Zhi Gu(顾长志), Lian-Feng Sun(孙连峰)

Chin. Phys. B . 2018, 27(12): 128101 . **doi:** 10.1088/1674-1056/27/12/128101

Modulated thermal transport for flexural and in-plane phonons in double-stub graphene nanoribbons

Chang-Ning Pan(潘长宁), Meng-Qiu Long(龙孟秋), Jun He(何军)

Chin. Phys. B . 2018, 27(8): 088101 . **doi:** 10.1088/1674-1056/27/8/088101

Free-standing, curled and partially reduced graphene oxide network as sulfur host for high-performance lithium-sulfur batteries

Hui-Liang Chen(陈辉亮), Zhuo-Jian Xiao(肖卓建), Nan Zhang(张楠), Shi-Qi Xiao(肖仕奇), Xiao-Gang Xia(夏晓刚), Wei Xi(席薇), Yan-Chun Wang(王艳春), Wei-Ya Zhou(周维亚), Si-Shen Xie(解思深)

Chin. Phys. B . 2018, 27(6): 068101 . **doi:** 10.1088/1674-1056/27/6/068101

Thermal conduction of one-dimensional carbon nanomaterials and nanoarchitectures

Haifei Zhan(占海飞), Yuantong Gu(顾元通)

Chin. Phys. B . 2018, 27(3): 038103 . **doi:** 10.1088/1674-1056/27/3/038103

Electromechanical actuation of CNT/PVDF composite films based on a bridge configuration

Xiaogang Gu(谷孝刚), Xiaogang Xia(夏小刚), Nan Zhang(张楠), Zhuojian Xiao(肖卓建), Qingxia Fan(范庆霞), Feng Yang(杨丰), Shiqi Xiao(肖仕奇), Huiliang Chen(陈辉亮), Weiya Zhou(周维亚), Sishen Xie(解思深)

Chin. Phys. B . 2017, 26(7): 078101 . **doi:** 10.1088/1674-1056/26/7/078101

A new sulfur-doped source and synergistic effect with nitrogen for carbon dots produced from glucose*

Lige Fu(付丽歌)[1], Yuehong Yin(殷月红)[1,†], Guohua Cao(曹国华)[1,‡], Pingping Wu(武苹苹)[1], Jian Wang(汪舰)[1], Lingling Yan(闫玲玲)[1], Baoqing Zhang(张宝庆)[2], and Ming Li(李明)[1]

[1] *School of Physics and Electronic Information, Henan Polytechnic University, Jiaozuo* 454000, *China*
[2] *School of Materials Science and Engineering, Henan Polytechnic University, Jiaozuo* 454000, *China*

(Received 15 August 2019; revised manuscript received 29 September 2019; published online 29 November 2019)

The nitrogen and sulfur co-doped carbon dots (N, S-CDs) with increased luminescence were synthesized by a hydrothermal process in one green pot by using glucose, and a new sulfur-doping source of sodium sulfite was developed. The synergistic effect of the N and S groups was well discussed through the structure analysis of Fourier transform infrared spectra and x-ray photoelectron spectra. The surface states of N, S-CDs embody more complicated functional groups, and S element exists as –SSO_3, –C–SO_3, and SO_4^{2-} groups due to the introduction of sodium sulfite. The sulfur-containing groups passivate the surface of the CDs, and the relatively high sulfur groups may reduce the non-radiation centers. The fluorescence is affected by the hydroxyl group of the solvent. The quenching of Fe^{3+} ion to fluorescence and the sensitivity of fluorescence to pH were also investigated.

Keywords: carbon dots, glucose, sodium sulfite, nitrogen and sulfur codoping, synergistic effect

PACS: 81.05.U–, 81.07.–b, 42.70.–a **DOI:** 10.1088/1674-1056/ab5213

1. Introduction

Fluorescent carbon dots (CDs) have received increasing attention due to their outstanding optical properties, good biocompatibility, low toxicity, and low cost, and have shown a wide range of applications, including bio-imaging, photocatalysis, metal detection, and opt-electric devices.[1–5] Until now, many methods have been explored for fabricating the fluorescent CDs,[6] such as the hydrothermal method, microwave methods, electrochemical oxidation, and carbonizing organic routes.[7–10] Although great progress has been made in the research of CDs, the luminescence mechanism is still not well addressed. The moderate growth process of CDs by the hydrothermal method is more conducive to understanding the luminescence mechanism.

The CDs of the same size prepared with different raw materials of synthesis always exhibit quite different fluorescence (FL) phenomena. The compositions and structures of CDs are the key factors to understand their complicated luminescence mechanisms,[11,12] which can be adjusted by doping other non-metallic elements or surface passivation.[13–17] The poly-aromatic structures can be induced by the N-doping, which will improve the quantum yield (QY) of the CDs, and the tunable luminescence has been obtained by adjusting the N contents.[18–20] Many groups reported that some organic ammonium compounds, such as primary amines and amino acids, can serve as surface modifiers for CDs.[21–24] Yang *et al.* prepared highly fluorescent N-doped CDs with QY 85% and discussed the chemical structure from citric acid and ethylenediamine (EDA).[25] Besides the fluorescence of CDs has been improved by nitrogen doping, much effort has been devoted to the development of CDs for practical application. Recently, the multi-element doped carbon dots have been developed, which are mainly doped with a combination of N and other elements, such as P, S, or B, and show higher luminous efficiencies.[18,21,26,27] Among them, the N, S-coped CDs (N, S-CDs) exhibit excellent photoluminescent properties, low cytotoxicity, and sensitivity.[28,29] By far, the sulfur and nitrogen sources often come from an organic substance, such as thiourea,[30] cysteine,[28] and so on. Although the performance of CDs may be improved by N, S-codoping, it is still a challenge to study the mechanism of the hetero atom doping on the fluorescence of CDs, especially the synergistic effects in the case of multi-element coexistence.[25] Meanwhile, it is the key factor to search for the fluorescence origin of the CDs.[31,32] Comparing with the organic sulfur source, the inorganic sulfur has better solubility in water and wider application. What is more important, it is simple and controllable to understand the effect of sulfur on the performance of CDs. Few studies have been reported on the inorganic materials as the sulfur source. In this paper, sodium sulfite as a new provider of sulfur atoms is reported. The N-doped CDs were synthesized from glucose and aqueous ammonia by ultrasonic method,[33] but the research of synergistic effects on the co-

*Project by the National Natural Science Foundation of China (Grant Nos. 51571085, 11805052, and 61705062), the Research Project for Basic and Forefront Technology of Henan Province, China (Grant No. 162300410219), and the Doctor Foundation of Henan Polytechnic University, China (Grant No. B2014049).

†Corresponding author. E-mail: yuehongyin@126.com
‡Corresponding author. E-mail: ghcao@hpu.edu.cn

© 2019 Chinese Physical Society and IOP Publishing Ltd

doped CDs needs to be carried out. We explore a green and facile synthesis of N, S-CDs by a one-step hydro-thermal treatment using glucose as the carbon source. The fluorescence properties of un-doped and doped CDs were investigated, and the composition structure and the synergistic mechanism of N, S co-doped CDs were discussed.

2. Experimental details

2.1. Preparation of carbon dots

Glucose (Glu, AR, 99.5%), ethylenediamine (EDA, AR, 99.0%), and sodium sulfite (Na_2SO_3, AR, Aladdin, 98.0%) were purchased from Aladdin Chemistry Co., Ltd. (Shanghai, China). All reagents were used without further purification. The pH of the solution was adjusted with sodium hydroxide (AR, 96.0%).

For preparing glucose-based carbon dots, the typical procedure was conducted. The un-doped CDs (G-CDs) were synthesized directly from glucose as the carbon source. 0.36 g of glucose was dissolved in 10 mL distilled water to obtain a dispersion solution, and then the solution was transferred to a 100 mL teflon liner. A hydro-thermal procedure was applied at 140 ℃ for 5 h. After the autoclave cooled to room temperature, the obtained liquid was dialyzed for 48 h in a dialysis bag having a molecular weight cutoff of 1000 Da (the deionized water was changed every 6 h). For the doping CDs, parallel experiments were carried out as follow: EDA as the nitrogen doping source for N-doped CDs (N-CDs), sodium sulfite as the sulfur doping source for S-doped CDs (S-CDs), EDA and sodium sulfite for N, S co-doped CDs (N, S-CDs). More details are listed in Table 1.

Table 1. Compositions of different raw materials.

	Glucose/g	EDA/g	Na_2SO_3/g	Water/ml
CDs	0.36	0	0	10
N-CDs	0.36	0.12	0	10
S-CDs	0.36	0	0.252	10
N, S-CDs	0.36	0.12	0.252	10

2.2. Structure characterization and performance testing

Transmission electron microscopy (TEM) and high-resolution transmission electron microscopy (HRTEM) measurements were performed on an electronic microscope (FEI Talos F200X). Fourier transform infrared (FT-IR) spectroscopy of the CDs was recorded by Nicolet 460 FT-IR spectrometer (Thermo Nicolet, USA). The x-ray photoelectron spectra were analyzed using Escalab 250XI (Thermo Fisher). The x-ray diffraction (XRD) patterns were recorded on a Shimadzu XRD-6000 powder x-ray diffractmeter. The fluorescence spectrum and the fluorescence lifetime were recorded by a steady transient fluorescence spectrometer and a transient spectrum (Fluorolog-3, HORBIA Scientific). The absolute photoluminescence quantum yield was measured by an integrating sphere attached to a Horiba Jobin Yvon fluororomax-4 spectro-fluorometer. All absorption spectra were measured by an ultraviolet–visible–near infrared spectrophotometer (UV-3600, SHIMADZU). Different pH solutions (3, 5, 7, 9, 11, 13) were prepared with 2 wt.% NaOH and dilute sulfuric acid.

3. Results and discussion

Figure 1 shows the UV–visible absorption spectrum and fluorescence emission spectrum of the CDs solution. There is an obvious excitation absorption peak at 272 nm, which comes from the π–π^* transition of C=C. At the same time, a small shoulder absorption peak at 340 nm is observed, which comes from the n–π^* transition of the C=O group in the un-doped CDs. However, the small shoulder absorption peak is not found in the S-CDs spectrum. Both N-CDs and N, S-CDs exhibit a wide absorption band, and they include two main absorption peaks at 350 nm and 270 nm. It is noted that a more obvious absorption peak at 270 nm is found in N, S-CDs, indicating that the CDs have both π–π^* and n–π^* transitions, and the former may be promoted by the interjection of sulfur atom. Figure 1(b) shows the fluorescence spectra of CDs at 380 nm excitation wavelength. The emission peaks are concentrated at around 460 nm, and comparing to other three CDs, there is a red shift (at 470 nm) of N-CDs. The fluorescence quantum yields (FLQY) of CDs measured by integrating spheres are 0.33% (G-CDs), 3.09% (S-CDs), 5.18% (N-CDs), and 6.31% (N, S-CDs), respectively. The fluorescence of the CDs is significantly improved by element doping, and compared with the FLQY of N-CDs, that of N, S-CDs is increased by 22%. The synthesized N, S-CDs emit bright blue light and the emission peaks have hardly shifted by changing the molar ratio of the raw materials. In order to explore the optical properties of the CDs, the fluorescence emission spectra of N, S-CDs at different excitation wavelengths were assessed. From Fig. 1(c), when the excitation wavelength increases from 300 nm to 500 nm, it can be seen that the fluorescence emission intensity of the CDs increases initially and decreases afterwards, and the maximum emission intensity can be obtained when excited at 360 nm. Furthermore, the fluorescence emission peak shifts from 417 nm to 557 nm with the longer excitation wavelength. Due to the surface defect state and the quantum confinement effect, the fluorescence emission of CDs often has significant excitation wavelength dependence.[34]

The micro-morphology of the CDs was characterized by TEM and XRD spectra. Figure 2(a) shows the TEM image of the obtained N, S-CDs. These small CDs are well dispersed with a diameter of about 5 nm. The HRTEM result (the inset of Fig. 2(a)) shows the lattice fringes with an average interplanar spacing of 0.29 nm, which is very close to the (002) diffraction faces of graphite.[28,35] Figure 2(b) displays the XRD pat-

terns of G-CDs, N-CDs, S-CDs, and N, S-CDs. The XRD patterns of the CDs show very broad diffraction peaks without other diffraction peaks, indicating that the CDs are less crystalline due to the highly disordered carbon atoms in the interior. G-CDs and N-CDs show the diffraction peaks at about $2\theta = 18.3°$. The peak shifts to about $2\theta = 20.7°$ in S-CDs and N, S-CDs. According to the diffraction principle, the interplanar spacing of the N, S-CDs is about 0.31 nm, which is a little larger than the result of HRTEM owing to the organic groups on the surface of the CDs.

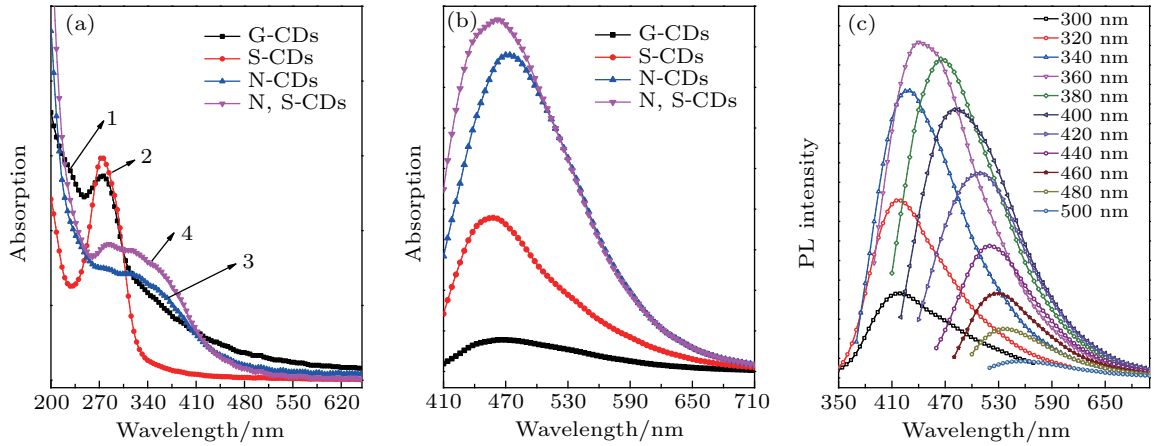


Fig. 1. (a) UV–vis absorption spectra and (b) fluorescence spectra ($\lambda_{ex} = 380$ nm) of G-CDs, S-CDs, N-CDs, and N, S-CDs dispersed in water. (c) Fluorescence spectra of N, S-CDs under varied excitation wavelengths.

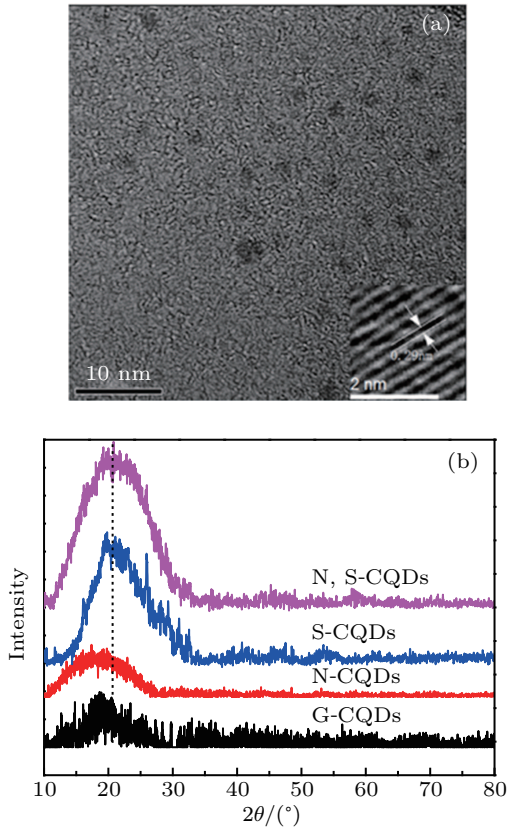


Fig. 2. (a) TEM and HRTEM images of N, S-CDs and (b) XRD patterns of G-CDs, S-CDs, N-CDs, and N, S-CDs.

To investigate the fluorescence emission mechanism, the surface functional groups of the four-type CDs were characterized by FTIR spectroscopy, and the result is shown in Fig. 3(a). The strong absorption bands at around 3420 cm^{-1} and 1594 cm^{-1} correspond to the stretching vibrations of O–H/N–H and C=O, respectively. The saturation vibration absorption of C–H, which is the inherent group of glucose, is detected at 2935 cm^{-1}. The surfaces of G-CDs, N-CDs, S-CDs, and N, S-CDs are rich in hydroxyl and carboxyl groups. These functional groups coincide with the excellent aqueous dispersivity. The C–N stretching vibration band at 1335 cm^{-1} is detected in N-CDs and N, S-CDs, which is consistent with the primary amide absorption. A large content of energy potential well of the amide contributes to the fluorescence generation. A new band at 1200 cm^{-1} arises from the stretching vibration of O=S=O, which confirms that sodium sulfite molecules are graphed onto the S-CDs and N, S-CDs surfaces. At the same time, both of them have obviously complex absorption bands in the fingerprint region of the FTIR spectrum. There are primary four stretching vibration peaks of C–O, C–S, $–SO_3H$, and C–H bonds, which indicates the existence of the sulfur-containing groups on the surface of N, S-CDs and the surface passivation caused by the entry of sodium sulfite. This result is in good agreement with the slight shift of the XRD diffraction peak.

The surface chemistry of N, S-CDs was further investigated by XPS. Four peaks appear at 285 eV, 399 eV, 532 eV, and 163 eV in the full scan spectrum as shown in Fig. 3(b), and their binding energies correspond to C 1s, N 1s, O 1s, and S 2p, respectively. The atomic percentages of N and S are 16.9% and 5.53%, which are consistent with the results obtained by FTIR and conform the formation of N, S-CDs. Figure 3(c) shows a high-resolution C 1s spectrum that can be deconvoluted to four component peaks with binding energies at 284.1 eV, 284.9 eV, 285.3 eV, and 287.3 eV, which are assigned to C–C, C–O, C–N, and C=O groups, respectively. The high-resolution spectrum of N 1s can be resolved into three

component peaks as shown in Fig. 3(d), which are assigned to pyridinic–N (398.9 eV), pyrrolic–N (400.8 eV), and N–O (397.1 eV) groups, respectively. Similarly, the high-resolution spectrum of O 1s can be deconvoluted to three component peaks in Fig. 3(e), suggesting that there are C=O (530.8 eV), C–O–C (531.7 eV), and O–H (534.8 eV) groups on the surface of the N, S-CDs. The high resolution fitting spectrum of S 2p is shown in Fig. 3(f) and the sulfur element exists in a plurality of states. The binding energy of 161.6 eV corresponds to the –SSO_3 group, and that of 162.8 eV corresponds to the –C–S– group, while the binding energies of 167.3 eV and 168.5 eV correspond to the –SO_4 and the –C–SO_3– groups, respectively. This is also in good agreement with the FTIR. Based on the analysis of FTIR and XPS, the surface states of N, S-CDs embody more complicated functional groups, the formation of the sulfur-containing group may passivate the surface of the CDs, and the relatively high sulfur groups may reduce the non-radiation centers.

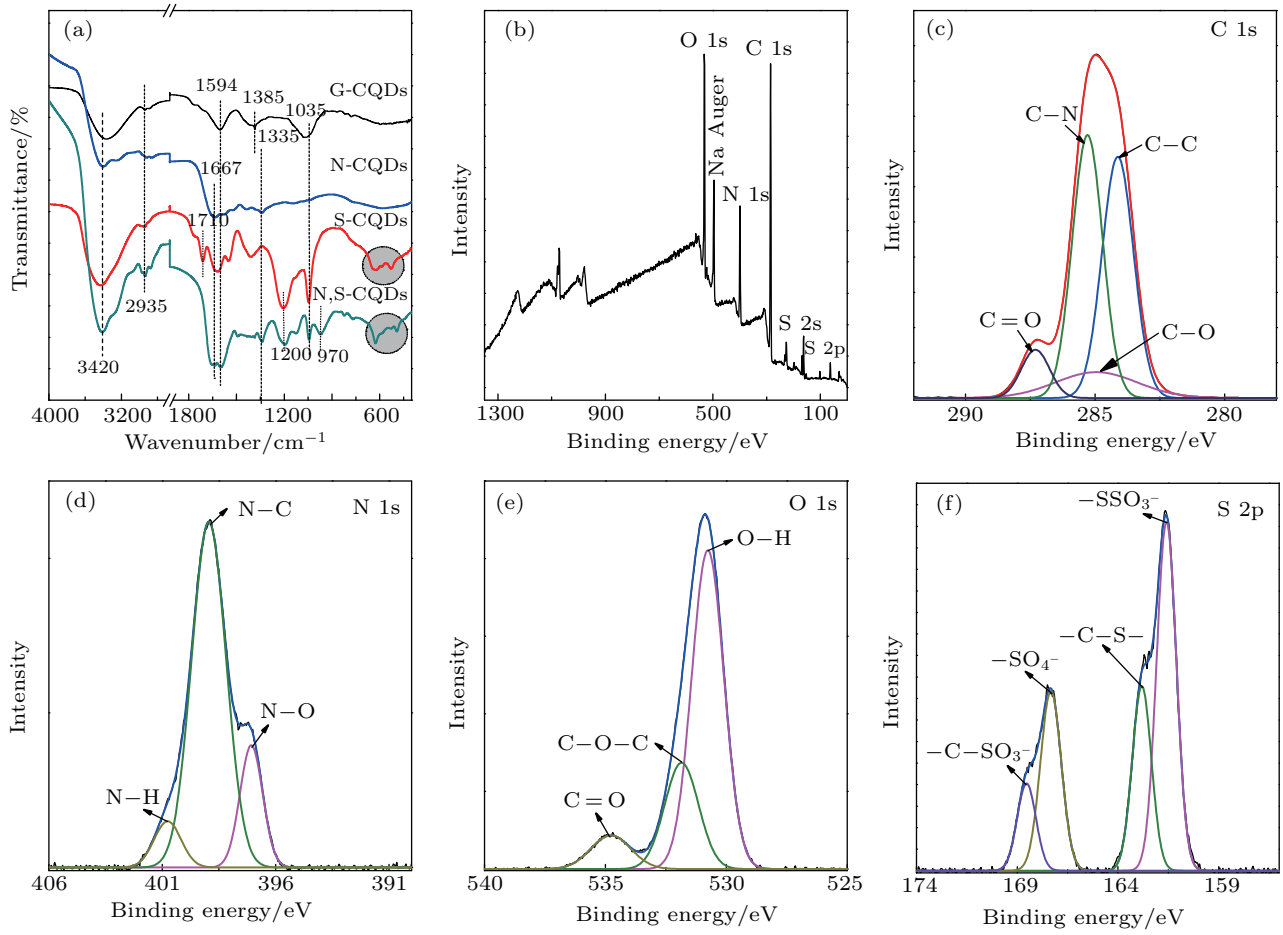


Fig. 3. (a) FT-IR spectra of G-CDs, S-CDs, N-CDs, and N, S-CDs and (b) XPS spectra of N, S-CDs. (c)–(f) High- resolution XPS data of C 1s, N 1s, O 1s, and S 2p of N, S-CDs.

To further investigate the origin of the CD fluorescence, fluorescence decay curves (excitation wavelength: 370 nm) of four-type CDs emissions were measured and demonstrated in Fig. 4 and Table 2. The fluorescence lifetime of G-CDs, N-CDs, S-CDs, and N, S-CDs was determined according to an established method with the following equation:

$$\tau = \frac{\sum \alpha_i \tau_i^2}{\sum \alpha_i \tau_i},$$

where τ_i is the fitted fluorescence lifetime, τ is the fitted average fluorescence lifetime, and α is the fitting coefficient.

A three-exponential fit was performed on the decay curves of G-CDs and N-CDs. For the G-CDs, it can be found that $\tau_1 = 3.28$ ns, $\tau_2 = 9.48$ ns, $\tau_3 = 0.87$ ns, and their proportions are 34.5%, 62.2%, and 3.3%, respectively. The average lifetime (τ) of G-CDs is 3.6 ns. The values of N-CDs are $\tau_1 = 3.59$ ns, $\tau_2 = 0.93$ ns, $\tau_3 = 10.32$ ns, and the average lifetime (τ) is 5.56 ns. The proportion of τ_3 increases to 9.5% comparing with that of G-CDs. When the single N element is doped, more surface states are introduced,[5] and then there are more fluorescent emissions from the surface defect state, resulting in that the fluorescence lifetime is relatively longer. The two-exponential fits were performed on the fluorescence lifetime of S-CDs and N, S-CDs. The fluorescence lifetime for S-CDs is $\tau_1 = 1.5$ ns, $\tau_2 = 4.69$ ns, and the average lifetime is 2.76 ns, while that of N, S-CDs is $\tau_1 = 1.4$ ns, $\tau_2 = 6.8$ ns, and the average lifetime is 2.9 ns. Comparing with the fluorescence lifetime of S-CDs, the proportion of τ_1 in N, S-CDs

is increased from 82.7% to 92.7%. The lifetime of N, S-CDs and S-CDs is lower than that of N-CDs. The surface of carbon dot may be passivated due to the introduction of sulfur, and the synergistic effect of nitrogen and sulfur promotes the emission from the surface molecular state and shortens the fluorescence lifetime of the CDs.

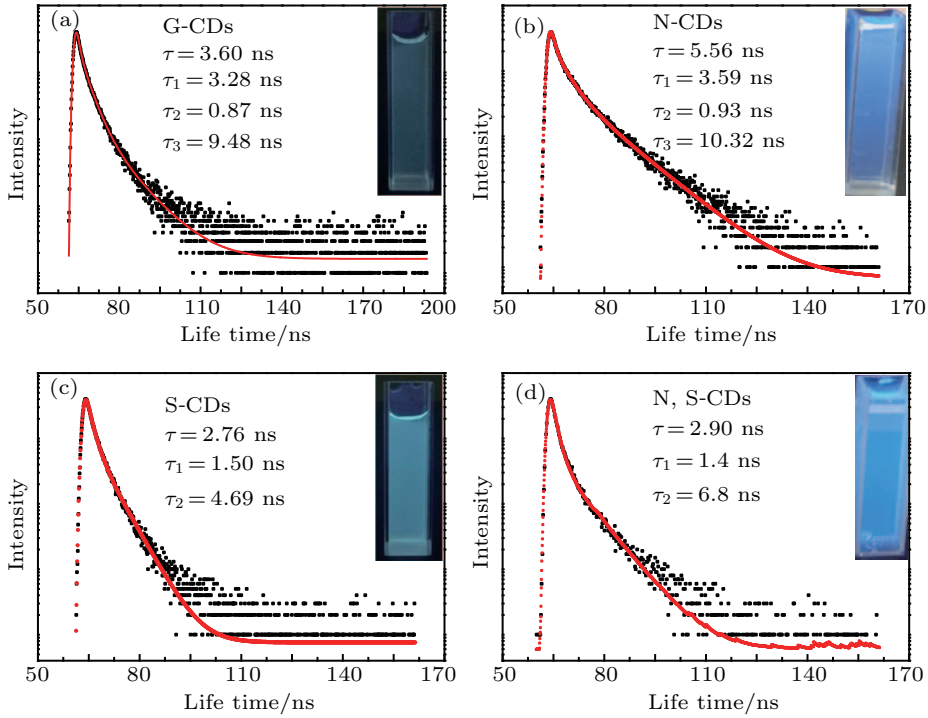


Fig. 4. Time-resolved fluorescence decay curves for (a) G-CDs, (b) N-CDs, (c) S-CDs, and (d) N, S-CDs in water (λ_{ex} = 360 nm).

Table 2. Biexponential fit values of the life time for G-CDs, N-CDs, S-CDs, and N, S-CDs in water.

	τ_1/ns	α_1/%	τ_2/ns	α_2/%	τ_3/ns	α_3/%	τ/ns
G-CQDs	3.28	34.5%	0.87	62.2%	9.48	3.30%	3.60
N-CQDs	3.59	28.4%	0.93	62.1%	10.32	9.5%	5.56
S-CQDs	1.50	82.7%	4.69	17.3%			2.76
N, S-CQDs	1.42	92.7%	6.81	7.3%			2.90

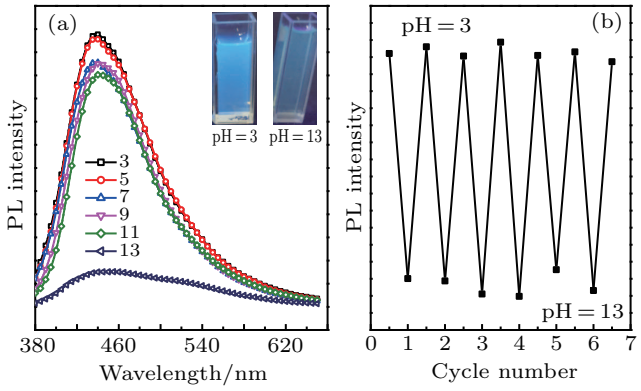


Fig. 5. (a) Fluorescence emission spectrum of N, S-CDs with various pH from 3 to 13; the insert is the photos under pH 3 and 13, respectively. (b) PL intensity upon the cyclic switching of N, S-CDs under alternating conditions of pH = 3 and pH = 13.

The pH sensitivity of the fluorescent carbon dots was also investigated. Figure 5(a) shows a fluorescence emission spectrum of the aqueous solution of N, S-CDs at different pH values. It can be seen that the fluorescence intensity of the carbon dots is affected by the pH value. The emission peak has hardly any shift when pH changes from 3 to 13. The fluorescence intensity is only slightly reduced in the pH range of 3–11, and the quenching effect is not obvious. However, a significant decrease of intensity is observed with a relatively fast rate within pH 11–13. As can be seen from the two comparative photographs of pH values of 3 and 13 inserted in Fig. 5(a), a significant quenching effect is obtained; it appears that the fluorescence intensity of the CDs is very sensitive to the strong alkaline solution. At the same time, we also studied the reversibility of the fluorescence switching operation upon variation of pH. The N, S-CDs are subjected to pH cycling between pH = 3 and pH = 13 using acid and base as modulators. As shown in Fig. 5(b), the fluorescence intensity can be restored and the switching operation can be repeated for six consecutive cycles, which indicates that the two-way switching process has good reversibility. The luminescence will be affected by pH, mainly because the surface of the fluorescent carbon dots contains hydroxyl or the carboxyl groups. Due to the change of pH, the hydroxyl group on the surface of the carbon dots adsorbs H^+, and the degree of dissociation of the carboxyl group is also affected when the pH value changes. There is a large amount of negative charge on the surface of carbon dots, which affects the fluorescence performance.[5,36]

To check the selectivity of this fluorescence system, we investigated the fluorescence quenching effect of various metal ions on the CDs. The metal ions included K^+, Mg^{2+}, Cu^{2+},

Al^{3+}, Cd^{2+}, Ca^{2+}, Zn^{2+}, and Fe^{3+}, and each with a concentration of 0.01 mol·L^{-1} was added into a CDs dispersion (0.001 mg·mL^{-1}). In Figs. 6(a) and 6(b), there is no obvious fluorescence quenching for K^+, Mg^{2+}, Cd^{2+}, Al^{3+}, Ca^{2+}, and Zn^{2+} ions; the visible fluorescence quenching can be observed for Cu^{2+} ions; and the strongest fluorescence quenching is obtained for Fe^{3+} among all the metal ions tested. The possible mechanism of the specific fluorescence quenching effect is the strong interactions between Fe^{3+} ions and the surface groups of N, S-CDs, such as hydroxyl or carboxyl groups, which can form complexes and transfer the photoelectrons from the CDs to Fe^{3+} ions.[28,32] Figure 6(c) shows the fluorescence spectra of the N, S-CDs solution containing different concentrations of Fe^{3+} at the excitation wavelength of 360 nm and a gradual decrease of the fluorescence intensity is found with the increase concentration of Fe^{3+}. There is a good linearity between the quenching efficiency (F/F_1) and the concentration of Fe^{3+} ions in the range of 20–600 μM with a correlation coefficient (R^2) of 0.998 in Fig. 6(d). Therefore, the concentration of Fe^{3+} could be calculated using the following calibration equation:[37]

$$\mathrm{Log}(F_0/F_1) = -0.00254 + 3.8199 \times 10^{-4} C,$$

where F_1 and F represent the fluorescence emission intensities of N, S-CDs in the presence and absence of metal ions, respectively, and C represents the concentration of Fe^{3+}. The limit of detection is estimated to be 2.355 μM at an S/N of 3. This result suggests that Fe^{3+} can be effectively detected with CDs via luminescence measurements in a narrow range of detection concentrations.

In summary, the fluorescence of CDs is significantly improved by element doping. The introduction of sulfur source does not produce a new luminescence center. There are obviously complex absorption bands in the fingerprint region and more complicated sulfur-containing functional groups, such as $–SSO_3$, $–SO_4$, and $–C–SO_3–$ groups. The sulfur-containing groups may passivate the surface of N, S-CDs, and the relatively high sulfur groups may reduce the non-radiation centers. So the synergistic effect of nitrogen and sulfur promotes the emission from the surface molecular state and improves the fluorescence quantum yield of CDs.

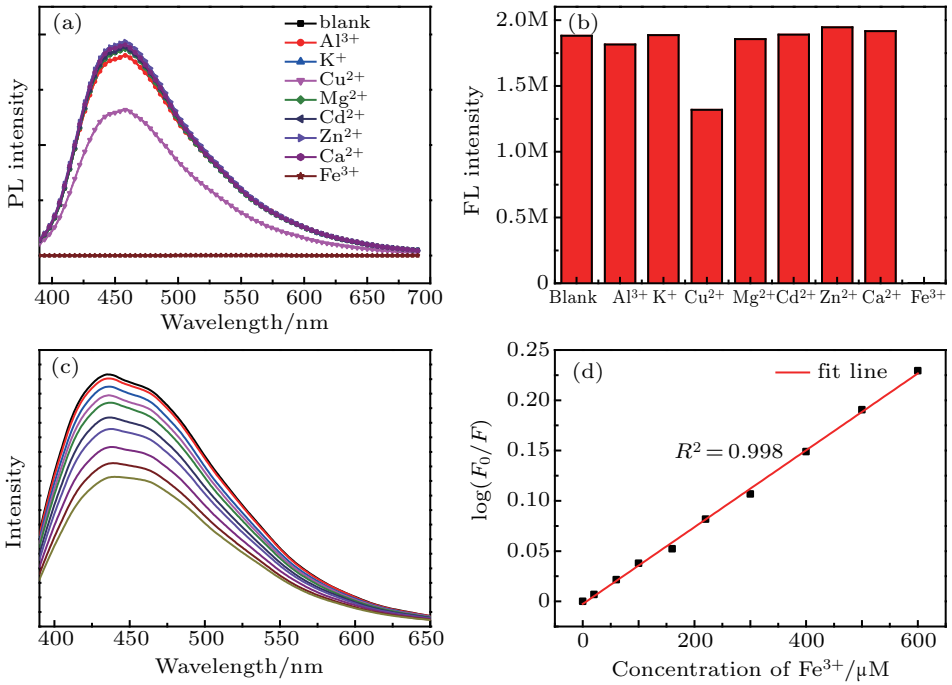


Fig. 6. (a) Fluorescence quenching and (b) comparison of fluorescence intensities of CDs after the addition of different metal ions. (c) Fluorescence quenching in the presence of Fe^{3+} ions (from top to bottom: 0, 20, 60, 100, 160, 220, 300, 400, 500, and 600 μM) and (d) relationship between the PL intensity and C-dots size and the concentration of Fe^{3+} ions.

4. Conclusion

Nitrogen, sulfur co-doping CDs were prepared by one-step hydro-thermal synthesis method using sodium sulfite as sulfur source and glucose as carbon source. According to the absorption spectra and fluorescence lifetime measurement, the origin of fluorescence from the surface molecular state was confirmed. The S element doping can passivate the surface state of the carbon dots, and the synergistic effect of nitrogen–sulfur co-doping improves the fluorescence performance of the CDs comparing with single N or S doping. The carbon dot shows good water solubility due to the carboxyl and hydroxyl groups on the surface. Our research indicates that the N, S-CDs have significant application in Fe^{3+} ion and strong alkaline solution detection.

References

[1] Wang Y and Hu A 2014 *J. Mater. Chem. C* **2** 6921
[2] He P, Yuan F, Wang Z, Tan Z and Fan L 2018 *Acta Phys.- Chim. Sin.* **34** 1250
[3] Qu D, Zheng M, Zhang L, Zhao H, Xie Z, Jing X, Haddad R E, Fan H and Sun Z 2015 *Sci. Rep.* **4** 5294
[4] He G, Shu M, Yang Z and Ma Y 2017 *Appl. Surf. Sci.* **422** 257
[5] Monoj K B, Bikash J, Santanu B and Amitava P 2014 *J. Phy. Chem. C* **118** 20034
[6] Guo Y, Wang Z, Shao H and Jiang X 2013 *Carbon* **52** 583
[7] Baker S N and Baker G A 2010 *Angew. Chem. Int. Edit.* **49** 6726
[8] Ming H, Ma Z, Liu Y, Pan K, Yu H, Wang F and Kang Z 2012 *Dalton Trans.* **41** 9526
[9] Zhu J, Bai X, Bai J and Pan J 2018 *Nanotechnology* **29** 085705
[10] Li Y, Zhao Y, Cheng H, Hu Y, Shi G, Dai L and Qu L 2012 *J. Am. Chem. Soc.* **134** 15
[11] Zhang D, Lin L Z and Zhu J 2014 *Chin. Phys. Lett.* **31** 28102
[12] Lan S, Li K and Gao X Y 2017 *Acta Phys. Sin.* **66** 136801 (in Chinese)
[13] Yang Z, Li X and Wang J 2011 *Carbon* **49** 5207
[14] Shan X, Chai L, Ma J, Qian Z, Chen J and Feng H 2014 *Analyst* **139** 2322
[15] Ye Q, Yan F, Shi D, Ye Q, Yan F, Shi D, Zheng T, Wang Y, Zhou X and Chen L 2016 *J. Photoch. Photobio. B* **162** 1
[16] Yang G, Wan X, Su Y and Zeng X 2016 *J. Mater. Chem. A* **4** 12841
[17] Yang Z, Wang M, Yong A M, Yang Z, Wang M, Marie A, Zhang X, Tan H, Chang Y, Li X and Wang J 2011 *Chem. Commun.* **47** 11615
[18] Qian Z, Ma J, Shan X, Feng H, Shao L and Chen J 2014 *Chem-Eur. J.* **20** 2254
[19] Zhang Y, Ma D, Zhuang Y, Zhang X, Chen W, Hong L, Yan Q, Yu K and Huang S 2012 *J. Mater. Chem.* **22** 16714
[20] SarithaDevi H V, Swapna M S, Ambadas G and Sankararaman S 2018 *Chin. Phys. B* **27** 107702
[21] Kasprzyk W, Bednarz S and Bogdal D 2013 *Chem. Commun.* **49** 6445
[22] Zhai X, Zhang P, Liu C, Bai T, Li W, Dai L and Liu W 2012 *Chem. Commun.* **48** 7955
[23] Dong Y, Pang H, Yang H B, Guo C, Shao J, Chi Y, Li C M and Yu T 2013 *Angew. Chem. Int. Edit.* **52** 7800
[24] Zhang Y, Tran R T, Qattan I S, Tsai Y T, Tang L, Liu C and Yang J 2013 *Biomaterials* **34** 4048
[25] Song Y, Zhu S, Zhang S, Fu Y, Wang L, Zhao X and Yang B 2015 *J. Mater. Chem. C* **3** 5976
[26] Zhou J, Shan X, Ma J and Gu Y 2014 *RSC Adv.* **4** 5465
[27] Wang G, Liu J, Dong W, Yan C and Zhang W 2018 *Acta Phys. Sin.* **67** 238103 (in Chinese)
[28] Wu H, Jiang J, Gu X and Tong C 2017 *Microchim Acta.* **184** 2291
[29] Luo X, Zhang W, Han Y, Chen X, Zhu L, Tang W, Wang J, Yue T and Li Z 2018 *Food Chem.* **258** 214
[30] Liu T, Cui Z, Zhou J, Wang Y and Zou Z 2017 *Nanoscale Res. Lett.* **12** 375
[31] Sun D, Ban R, Zhang P, Wu G, Zhang J and Zhu J 2013 *Carbon* **64** 424
[32] Ma Z, Ming H, Huang H, Liu Y and Kang Z 2012 *New J. Chem.* **36** 861
[33] Xu Q, Pu P, Z hao J, Wan X, Zhen S and Huang C 2015 *J. Mater. Chem. A* **3** 542
[34] Zhan H and Gu Y 2018 *Chin. Phys. B* **27** 38103
[35] Mohammad A, Tooba H and Jamshid L 2014 *Spectrochim. Acta A* **122** 715
[36] Wei C, Li J, Xiao X, Yue T and Zhao D 2018 *RSC Adv.* **8** 20016
[37] Chen B, Xie H, Wang S, Guo Z, Hu Y and Xie H 2019 *J. Nanopart. Res.* **21** 76